Electronic Analysis of Pulse Propagation

through an X-Ray Framing Camera

Jack Valinsky

Brighton High School

Rochester, New York

Advisers: Dr. William Donaldson & Dr. Dustin Froula

Laboratory for Laser Energetics

University of Rochester

Rochester, New York

November 2012

1. Abstract

Voltage pulses sent through x-ray framing cameras (XRFC's) used on the Omega laser system act as shutters, creating rapid time-delayed snapshots of a target during implosion with sub-nanosecond resolution. The program TOAST (Transmission line Optimization And Studying Tool) was written to model the propagation of a voltage pulse through the micro-channel plate (MCP) of an x-ray framing camera, which was treated as a transmission line. The current produced by the x-rays hitting the MCP was found to affect the voltage pulse; the sensitivity of the framing camera is therefore dependent on the intensity of the x-rays illuminating the MCP. Voltage reflections occur due to the incident x-rays changing the impedance of the MCP, distorting the time resolution of the camera. Simulation of the velocity of the voltage pulse allows for a more accurate determination of the time between snapshots. TOAST allows for a potential method of correcting XRFC images for distortions that is more accurate than flat-fielding.

2. Introduction

Nuclear fusion is a potential source of clean, sustainable energy that is under research and development in the United States and other countries. Energy is produced in nuclear fusion reactions by a process where lighter atomic nuclei fuse together to form a heavier nucleus. One such facility that is investigating the processes underlying nuclear fusion is the Laboratory of Laser Energetics (LLE) at the University of Rochester. Inertial confinement fusion is studied at LLE with the 60-beam OMEGA laser system by heating and imploding cryogenic targets. The small spherical plastic targets are filled with DT gas, a mixture of deuterium and tritium (isotopes of hydrogen), and chilled to cryogenic temperatures to form a layer of DT ice inside the target shell [1].

While heated uniformly with lasers, the outer plastic shell ablates outward as the contents of the target are imploded. The implosion of the deuterium and tritium results in conditions of high pressure and temperature. As a result of the high temperatures, positively charged nuclei of deuterium and tritium are able to overcome their repulsion forces and fuse together to form a helium nucleus and a high energy neutron. These neutrons comprise most of the energy released by the fusion reaction. High pressure conditions guarantee that a large number of fusion reactions occurs before the target explodes. Breakeven is achieved when the energy released by the fusion reactions is greater than the energy input of the lasers. Once high enough energy gain is achieved, laser fusion can be used as a viable source of energy [1].

X-rays are produced during the implosion of the target, which lasts approximately one nanosecond. Imaging devices like streak cameras and x-ray framing cameras (XRFC's) utilize this x-ray radiation to monitor the deformation of the target as it implodes. Streak cameras have a

time resolution that can be as short as one picosecond, which is much smaller than that of

XRFC's; however, they can only provide imaging in one dimension. This results in a great loss

of information. The resolution of XRFC's is limited by their frame rate to about 40 picoseconds,

but XRFC's produce two-dimensional images of the target during its implosion [2]. Uniform

compression is essential for maximum energy output [1].
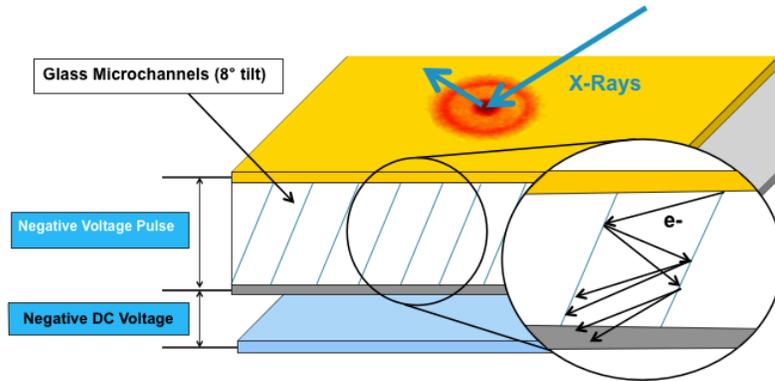
Fig. 1. Physical Diagram of an XRFC. *An XRFC consists of an MCP placed between two metal electrodes and a phosphor screen underneath. A negative voltage pulse is applied to two metal electrodes (gold and silver) and is propagated through the MCP. Positive voltage is applied to the surface of the phosphor screen.*

XRFC's consist of a doped-glass micro-channel plate (MCP) sandwiched between two

metal electrodes (top gold, bottom silver) and a phosphor screen (Fig. 1). Incoming x-rays from

the imploding target strike the top electrode and kick off electrons that hit a phosphor screen,

producing light. Collecting this light to form an image can be achieved with a film pack or a

CCD camera. A negative voltage pulse sent through the MCP acts as a shutter. When the pulse

passes through a section of the MCP, an electric field is generated that accelerates electrons down

the channels of the MCP.

Without the voltage pulse, few electrons reach the phosphor and only a dim image is

produced. The channels of the MCP are at an 8° tilt. As an electron travels down through the

MCP, it will strike the walls of a channel. With the added energy picked up by the electron from

accelerating through the electric field, more electrons can be kicked off the wall of the channel

when it hits. This causes an avalanche of electrons as each new electron picks up energy from the

electric field, knocking off more electrons. The cycle repeats down the length of the channel.

Positive DC voltage is applied to the phosphor screen to pull electrons off of the bottom electrode to develop an image [2].

An XRFC may be designed to take one or multiple images. Multiple images may be obtained by projecting several x-ray images across the MCP. However, only where the voltage pulse is currently passing through (and thus causing a gain in electrons) is the image strong enough to be captured by film or a CCD camera [2].

XRFC images must undergo post-processing due to distortions introduced by the MCP. The current method of correcting framing images, know as flat-fielding, takes a data image and divides it by an image produced by a uniform x-ray exposure at the same intensity. This method makes the assumption that the relationship between x-ray intensity and the recorded signal of the XRFC is linear. However, at a certain threshold intensity of x-rays one may get a 10% reduction in signal compared with the linear assumption; at higher x-ray intensities this would be more pronounced.

In this work, mathematical formulas and a computer program (TOAST) were developed to simulate the propagation of a voltage pulse through an XRFC. The simulation calculates the changes in voltage and current over an adjustable number of nodes across the MCP of an XRFC as a voltage propagates in the presence of a distribution of x-rays. Results from the simulation indicate that the relationship between x-ray intensity and the signal received by the camera is in fact nonlinear, thus showing that the underlying assumption in flat-fielding XRFC images is incorrect. The computer program allows for a potentially more accurate determination of the speed of the pulse through the MCP as well as correction of distortions in the images introduced by the camera itself.

3. Mathematical Model

3.1 *The XRFC*

For the purpose of simplicity, the model constructed in this project was one-dimensional, but it is sufficient to provide useful insight on the complex interactions that occur between the camera, incident x-rays, and propagated pulse. A transmission line was used to model an XRFC [3].
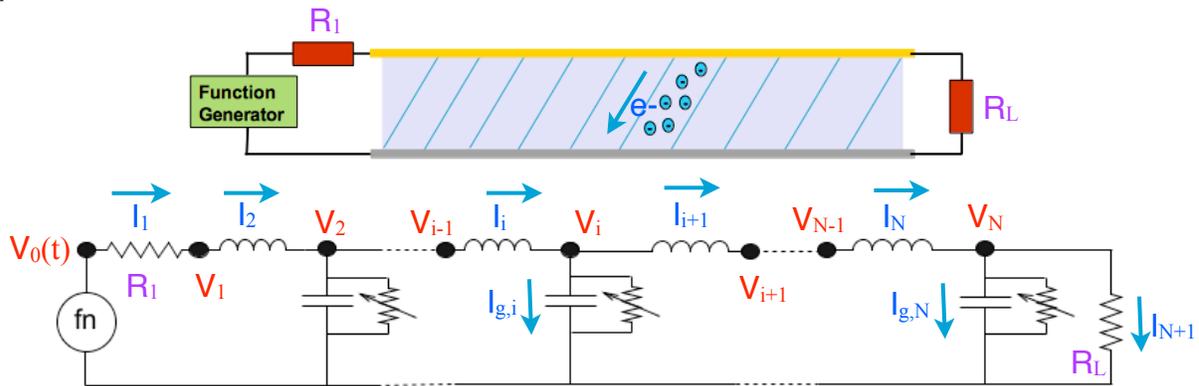
Fig. 2. Physical and Circuit Diagrams of an MCP.
There are two terminal resistances at the beginning and end of the MCP.
As x-rays strike the MCP, a current is produced that is modeled by a
variable resistance. Note that the circuit may have any number of nodes.

Parallel sheets of metal will produce a capacitance in the presence of electric current. The sheets of metal will have an inductance in the presence of an alternating current source (AC), such as a pulse. As shown in Fig. 2, the capacitances and inductances of the metal electrodes are modeled as capacitor and inductor pairs connected in a series/parallel combination [3]. Incident x-rays strip electrons from the surface of the top metal electrode and the electrons are then accelerated down the channels of the MCP by the electric field produced from the negative voltage pulse. This produces currents in the MCP as modeled by variable resistances. A transmission line is a circuit that allows for the propagation of a pulse. The MCP of the XRFC functions as a modified transmission line with the added reduction in current induced by an x-ray

source. Terminal resistances shown in the diagram are crucial, as shown later, for preventing

large voltage reflections at the ends of the MCP.

For this model, equations relating voltage and current of the discrete components for an AC

circuit are necessary to simulate the propagation of the voltange pulse [3]. The equations for a

resistor, capacitor, and inductor are given as follows:

$$V=IR \tag{1}$$

$$V=\frac{Q}{C}=\frac{\int Idt}{C} \tag{2}$$

$$V=L\frac{dI}{dt} \tag{3}$$

where V is voltage, I is current, R is resistance, Q is charge, C is capacitance, L is inductance,

and t is time [3]. Solving equation 1 in terms of I yields:

$$I=\frac{V}{R} \tag{4}$$

For equation 2, one must first take the derivative of both sides,

$$\frac{dV}{dt}=\frac{I}{C} \tag{5}$$

linearizing the derivative, then solving for I gives the form:

$$I=\frac{V-V'}{\Delta t}C \tag{6}$$

Dividing L from both sides of equation 3 and then integrating with respect to t gives the form of:

$$\int_{t'}^{t}\frac{V}{L}dt=\int_{I'}^{I}dI=I-I' \tag{7}$$

Using a trapezoid approximation for the integral and rearranging terms gives the equation:

$$I=\frac{1}{L}\left(\frac{V+V'}{2}\right)\Delta t+I' \tag{8}$$

Note that the substitutions dI=ΔI=(I-I') and dt=Δt were made. All prime values in equations

represent the previous time step. These equations are used to solve for current at each of the

nodes of the circuit modeling the XRFC. In the circuit diagram in Fig. 2, the nodes are given by the black dots. There are three type of nodes; the first node in between the terminal resistor R_1 and first inductor, all of the middle nodes (with units consisting of inductors, capacitors, and variable resistors), and the last node that is like a middle node with a terminal resistor R_L.

Applying Kirchoff's continuity law at each of the nodes (Fig. 2), three sets of equations are produced:

$$I_1 = I_2 \tag{9}$$

$$I_i = I_{g,i} + I_{i+1} \tag{10}$$

$$I_N = I_{g,N} + I_{N+1} \tag{11}$$

where I_1 is the current through the first terminal resistor, I_2 is the current through the first inductor, I_i is the current into node i from the previous inductor, $I_{g,i}$ is the current from node i through the current capacitor and resistor pair, I_{i+1} is the current from node i into the next inductor, I_N is the current into node N from the last inductor, $I_{g,N}$ is the current from node N into the last capacitor and resistor pair, and I_{N+1} is the current from node N into the last terminal resistor [3].

Substituting equations 4, 6, and 8 into equations 9, 10, and 11 yields:

$$\frac{V_0(t) - V_1}{R_1} = \frac{\Delta t}{2L}(V_1 - V_2 + V_1' - V_2') + I_2' \tag{12}$$

$$\frac{\Delta t}{2L}(V_{i-1} - V_i + V_{i-1}' - V_i') + I_i' = \frac{C}{\Delta t}(V_i - V_i') + I_{i+1}' + \frac{\Delta t}{2L}(V_i - V_{i+1} + V_i' - V_{i+1}') \tag{13}$$

$$\frac{\Delta t}{2L}(V_{N-1} - V_N + V_{N-1}' - V_N') + I_N' = \frac{C}{\Delta t}(V_N - V_N') + \frac{V_N}{R_L} \tag{14}$$

where $V_0(t)$ is the voltage from the pulse generator, R_1 is the first terminal resistor, R_L is the last terminal resistor, V_1 is the voltage from the first terminal resistor, V_2 is the voltage from the first inductor, V_i is the voltage at the current node, V_{i-1} is the voltage at the previous node, V_{i+1} is the

voltage at the next node, V_{N-1} is the voltage at the second to last node, and V_N is the voltage at the last node, which is also the voltage across the last terminal resistor [3]. At this stage the variable resistances of Fig. 2 used to model currents due to x-rays have not been included.

Finally, solving for voltage and rearranging equations 12, 13, and 14 so that all the current values are on one side and previous time steps are on the other gives:

$$\left(\frac{1}{R_1}+\frac{\Delta t}{2L}\right)V_1-\frac{\Delta t}{2L}V_2=-I_2{}'+\frac{V_0(t)}{R_1}-\frac{\Delta t}{2L}(V_1{}'-V_2{}') \qquad (15)$$

$$\left(\frac{\Delta t}{L}+\frac{C}{\Delta t}\right)V_i-\frac{\Delta t}{2L}V_{i-1}-\frac{\Delta t}{2L}V_{i+1}=I_i{}'-I_{i+1}{}'+\frac{C}{\Delta t}V_i{}'+\frac{\Delta t}{2L}(V_{i-1}{}'-2V_i{}'+V_{i+1}{}') \qquad (16)$$

$$-\frac{\Delta t}{2L}V_{N-1}+\left(\frac{1}{R_L}+\frac{\Delta t}{2L}+\frac{C}{\Delta t}\right)V_N=I_N{}'+\frac{\Delta t}{2L}(V_{N-1}{}'-V_N{}')+\frac{C}{\Delta t}V_N{}' \qquad (17)$$

In order to calculate the voltage for each node, Eqs. 15-17 show that the voltages and currents from the previous time step need to be known. At t=0, V' and I' are zero at each node. For the first step in the simulation, the only non-zero term on the right hand side of Eqs. 15-17 is $V_0(t)/R_1$. Solution of these equations provides the voltages at the end of this step. The currents at the end of this step are then obtained from Eq. 8. A bootstrap process occurs where these voltages and currents become the V' and I' values for the next time step.

Equations 15, 16, and 17 are a linear system of equations that can be written as a matrix equation:

$$[A][k]=[D] \qquad (18)$$

where A is a matrix containing all the coefficients on the left hand side of equations 15, 16, and 17; k is a column vector containing all the unknown voltages; and D is a column vector of the

constants on the right hand side of equations 15, 16, and 17 (previous time step) for each node.

The matrix equation is in the form:

$$
\begin{bmatrix}
b_1 & c_1 & & & & 0 \\
a_2 & b_2 & c_2 & & & \\
& a_3 & b_3 & \ddots & & \\
& & & \ddots & \ddots & c_{N-1} \\
0 & & & & a_N & b_N
\end{bmatrix}
\begin{bmatrix}
V_1 \\ V_2 \\ V_3 \\ \vdots \\ V_N
\end{bmatrix}
=
\begin{bmatrix}
D_1 \\ D_2 \\ D_3 \\ \vdots \\ D_N
\end{bmatrix}
\tag{19}
$$

In the program TOAST, the fast and efficient tridiagonal matrix method was used to solve this equation. Tridiagonal matrices contain entries of 0 except for the main (b), super (c), and sub-diagonals (a). The matrix equation can be written in the form,

$$
a_i V_{i-1} + b_i V_i + c_i V_{i+1} = D_i \tag{20}
$$

Except for the first and last entries of the a, b, and c diagonals, an entry a_i contains the coefficient of V_{i-1}, an entry b_i contains the coefficient of V_i, and an entry c_i contains the coefficient of V_{i+1}. The entry b_1 contains the coefficient of V_1, c_1 contains the coefficient of V_2, a_{N-1} contains the coefficient of V_{N-1}, and b_N contains the coefficient of V_N. This is due to the fact that the equations for the first and last nodes (Eqs. 15 and 17) have only two variables.

As mentioned previously, Δt is the time step of numerical derivation for calculating the voltage values in the simulation of the XRFC for the program TOAST. Later on it will be shown to be the time step for numerical integration to calculate the raw XRFC image(s) of the simulation. It must be significantly smaller than the time delay constant (τ) of the transmission line ($\Delta t \ll \tau$). The time delay constant is the time at which the circuit will appear as it would at $t = \infty$. For example, at $t = \infty$ capacitors will appear to be breaks in the circuit and the voltage V_i will be seen across the last terminal resistor. The time delay constant is given by the equation:

$$
\tau_{TX\ Line} = \sqrt{LC} \tag{21}
$$

where L and C are inductances and capacitances per unit length Δx (distance between nodes) [4].

The characteristic impedance of the transmission line (Z_0) governs the velocity at which the voltage pulse can propagate through. Higher impedance results in a slower velocity, whereas lower impedance results in a faster velocity. For a stripline MCP, the experimentally derived equation is:

$$Z_0 = \frac{\eta_0}{\sqrt{\varepsilon_r}} \left[\frac{a}{b} + \frac{1.0}{\pi} \ln(4) + \frac{\varepsilon_r + 1.0}{\pi} \ln\left(\frac{\pi e \left(\frac{a}{b} + 0.94 \right)}{2.0} \right) + \frac{\varepsilon_r - 1.0}{2\pi\varepsilon_r^2} \ln\left(\frac{e\pi^2}{16.0} \right) \right]^{-1} \quad (22)$$

where η_0 is the impedance of free space (about 120π Ω), ε_r is the relative permittivity constant of the MCP dielectric (3.8 for glass), a is half the width (w) of the stripline, and b is half the height or thickness (h) of the stripline [5]. The relationship between the terminal resistances and the characteristic impedance of a transmission line is very important because when they are matched a pulse consisting of a perfect sine wave will have all of its energy absorbed completely by a terminal resistor. More energy being absorbed at the end of the line means a less powerful voltage reflection when the pulse hits the back of the line and rebounds. Voltage reflections can cause great distortions in XRFC images. A perfect sine wave is impossible to create and more complex shapes are required for an XRFC; however, closely matching terminal resistances to the characteristic impedance minimizes voltage reflections [4].

Capacitance (C_0) and inductance (L_0) of the transmission line (not per unit length) are related to the characteristic impedance by the equation:

$$Z_0 = \sqrt{\frac{L_0}{C_0}} \quad (23)$$

Capacitance of the transmission line is given by the equation:

$$C_0 = \frac{\varepsilon_r \sigma}{h} \quad (24)$$

where σ is the surface area of the MCP (width w multiplied by length λ of the MCP):

$$\sigma = \lambda w \qquad (25)$$

and ε is the absolute permittivity of the MCP dielectric calculated by the equation:

$$\varepsilon = \varepsilon_r \varepsilon_0 \qquad (26)$$

where ε_0 is the permittivity of free space. Substituting in equation 24 for C_0 and solving equation 23 for L_0 yields the equation for finding the inductance of the line:

$$L_0 = Z_0^2 \left(\frac{\varepsilon \sigma}{h} \right) \qquad (27)$$

Thus, the inductance per unit length or the inductance per node (L) is simply:

$$L = \frac{L_0}{\lambda} \qquad (28)$$

The induced currents from the incoming x-rays striking the MCP change the impedance of the line, thus continuously altering the velocity of the voltage pulse. Without the effects of the incoming x-rays, the velocity (v) of a voltage pulse propagating unhindered through a transmission line can be expressed as a relationship between the relative permittivity of the MCP dielectric (ε_r) and the speed of light (c): $\quad v = \dfrac{c}{\sqrt{\varepsilon_r}} \qquad (29)$

Finally, the voltage pulse itself was modeled by a simple square wave, although more complex pulse shapes can be and often are used. A super-gaussian equation was used to approximate a perfect square wave:

$$V_0(t) = V_0 \exp\left(-\left(\frac{t - t_0}{\tau_w} \right)^a \right) \qquad (30)$$

where V_0 is the maximum voltage of the pulse, t_0 is the halfway time of the pulse, τ_w is the pulse width, and a determines how "flat" and "square-like" the pulse is (a high a value is desired).

High voltage pulses are required for a gain to occur on the MCP of the XRFC. A pulse width of 50 ps and a time delay on the pulse of 50 ps from the start of the simulation were used.

3.2 *X-ray Gain and Induced Current*

As mentioned previously, the propagating voltage pulse produces a gain in the MCP. This is due to a negative electric field produced by the pulse that accelerates electrons through the channels of the MCP. These electrons gain enough energy to knock off more electrons from the walls of the channels, which are at an 8° tilt so that electrons will strike the walls more frequently. Throughout the channels of the MCP, the cycle of electrons gaining energy and kicking off more electrons creates an avalanche of electrons which is the source of the gain. The gain (G) of the MCP, defined as the number of electrons produced per x-ray photon, is given by the voltage to a power (x) multiplied by a constant of proportionality (k) [2]:

$$G = k(V^x) \tag{31}$$

From the Photonis material data sheets on their XRFC's, a power of 8.399 and a k value of $1.27064 \cdot 10^{-22}$ were determined [6]. The power is roughly the average number of times an electron would strike the walls of a channel in its path through the MCP [2]. The number of electrons (N_e) in a section of the MCP increases due to the x-ray flux and decreases as a result of electrons created by the avalanche leaving through the bottom surface of the MCP. It is governed by the following equation:

$$\frac{dN_e}{dt} = G\phi_{x-ray} - \frac{I_{x-rays}}{q_e} \tag{32}$$

where ϕ_{x-ray} is the number of x-ray photons incident per unit time, I_{x-rays} is the current leaving through the bottom of the MCP, and q_e is the charge of an electron. The x-ray flux is

related to the intensity (ψ) in Watts/cm^2 of incoming x-rays and the work function of the gold

electrode (W_{Au}):

$$\phi_{x-ray} = \frac{\psi p w \Delta x}{W_{Au}} \tag{33}$$

where $w\Delta x$ is the surface area of the node. Porosity (p) is included in the equation due to the fact

that the top metal electrode is not solid gold, but it is perforated to allow electrons generated at

the top of the electrode by incident x-rays to travel down into the channels of the MCP.

The current leaking through the node on the MCP is given by the equation:

$$I_{x-rays} = n_e q_e v (w\Delta x) \tag{34}$$

where n_e is the number of electrons per unit volume at the bottom of the MCP and v

is their final velocity after acceleration through the MCP (calculated below). In this model n_e is

approximated by N_e/δ, where δ (equal to $hw\Delta x$) is the volume of the node. This gives

$$I_{x-rays} = \frac{N_e q_e v}{h} \tag{35}$$

so that equation 32 becomes:

$$\frac{dN_e}{dt} = G\phi_{x-ray} - \frac{N_e v}{h} \tag{36}$$

This is integrated over a time step Δt to give

$$N_e = N_e' + \Delta t \left(G\phi_{x-ray} - \frac{N_e' v}{h} \right) \tag{37}$$

Equation 37 states that the current number of electrons at any time t is the number of

electrons that were in the node at the previous time step plus the number of electrons generated

by striking x-rays minus the number of electrons that have since left the node. Initially, N_e' is

equal to zero. In solving Eq. 37 care is taken to ensure that Δt is sufficiently small that N_e does

not become negative.

The current $I_{\text{x-rays}}$ is added to the current at a node from the propagating pulse. One consequence of this is that it steals energy from the voltage pulse. The voltage pulse under a section of the MCP that is illuminated by x-rays will be attenuated. To produce an image or signal (S) from the simulated XRFC, the $I_{\text{x-rays}}$ currents at each node are simply integrated for the time interval [a,b] of the simulation:

$$S= \int_a^b I_{x-rays}\, dt \tag{38}$$

To calculate the velocity v of the electrons leaving the MCP, note that the strength of the electric field (E) from the voltage pulse is related to the voltage at a node i (V_i) and the separation between electrodes (in this case the thickness h of the MCP) by the equation:

$$E= \frac{V_i}{h} \tag{39}$$

The force on an electron (F_e) from the E-field is related to q_e and the strength of the field:

$$F_e=q_e E \tag{40}$$

Applying Newton's second law of motion, one obtains the form:

$$F_e=q_e E=m_e a_e \tag{41}$$

where a_e is the acceleration of the electron due to the E-field and m_e is the mass of the electron. The mass of one electron is approximately $9.10938 \cdot 10^{-31}$ kg and the charge of one electron is $1.602177 \cdot 10^{-19}$ C. Solving for a_e yields the equation:

$$a_e= \frac{F_e}{m_e} \tag{42}$$

The distance traveled by a projectile is related to its initial velocity (v_0), acceleration (a_e), and time (t). The vertical distance traveled by an electron in a channel is thus given by:

$$d_y=v_0 t+ \frac{1}{2} a_e t^2 \tag{43}$$

After an electron has traveled down a portion of a channel, it is assumed that it will

lose all kinetic energy due to collisions with the wall so that the previous velocity v_0 is always zero. The average distance traveled by the electron is the quotient of the thickness h of the MCP divided by the average number of hits against the wall. From equation 31 the average number of hits is x, which is approximately 8.399. Substituting in for d_y:

$$\frac{h}{x} = \frac{h}{8.399} = \frac{1}{2}a_e t^2 \tag{44}$$

Now the equation can be solved for t:

$$t = \sqrt{\frac{2h}{8.399a_e}} \tag{45}$$

The final velocity can be calculated from the initial velocity, acceleration, and time:

$$v = v_0 + a_e t \tag{46}$$

Substituting in equation 45 for t yields:

$$v = \sqrt{\frac{2ha_e}{8.399}} \tag{47}$$

Equation 47 gives the velocity of an electron as it accelerates through the E-field created by the voltage pulse propagating through the MCP. This velocity is crucial for calculating the current through a node $I_{x\text{-rays}}$ induced by x-rays as mentioned above. The current feeds back into the transmission line equations (Eqs. 15-17) and the detected signal on the CCD camera depends on the total charge provided by this current.

Results
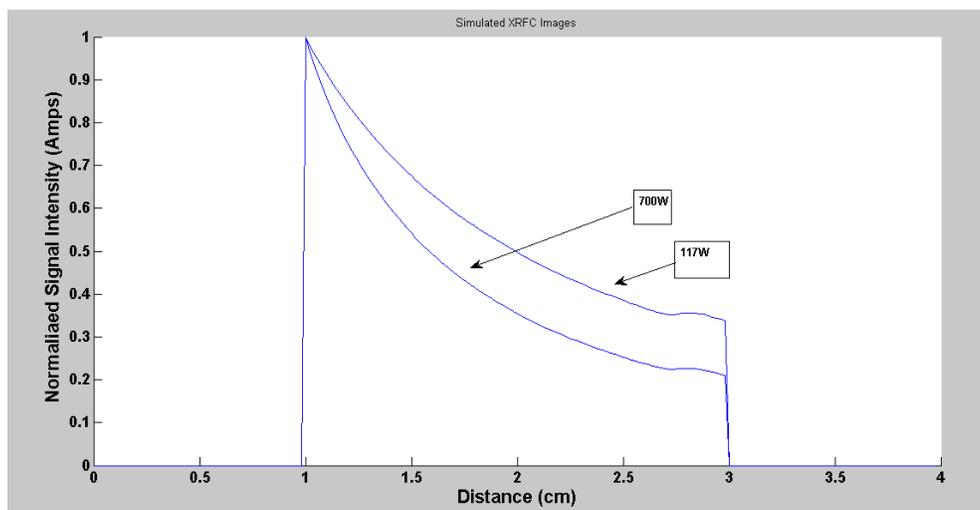
Fig. 3.
Time-integrated signal as a function of distance along an MCP calculated by TOAST, run at two different x-ray intensity levels, 700 and 117 W/cm². Notice the attenuation of the voltage pulse as it traveled through a portion of the MCP (1 cm to 3 cm) illuminated by x-rays. Higher intensity resulted in more attenuation.

Utilizing equation 38, graphs were calculated of the signal that a phosphor screen would see from a simulated XRFC in TOAST with the portion of the MCP from 1 cm to 3 cm uniformly illuminated by x-rays. Figure 3 shows two such graphs for different x-ray intensities, illustrating that attenuation of the voltage pulse occurred as it traveled through the portion of the MCP illuminated by x-rays. Experimental data taken from shot #64187 conducted on the OMEGA laser system [7] and shown in Fig. 4 agrees qualitatively with the simulation results. Two different exposures of an XRFC were done, both with a uniform source of x-rays. The first exposure was done with a normal flat-fielding exposure of x-rays. The second XRFC had a mask that only allowed a small sliver of x-rays to reach the MCP. This showed a much less attenuated signal as the pulse swept across the XRFC compared with the one with full exposure.
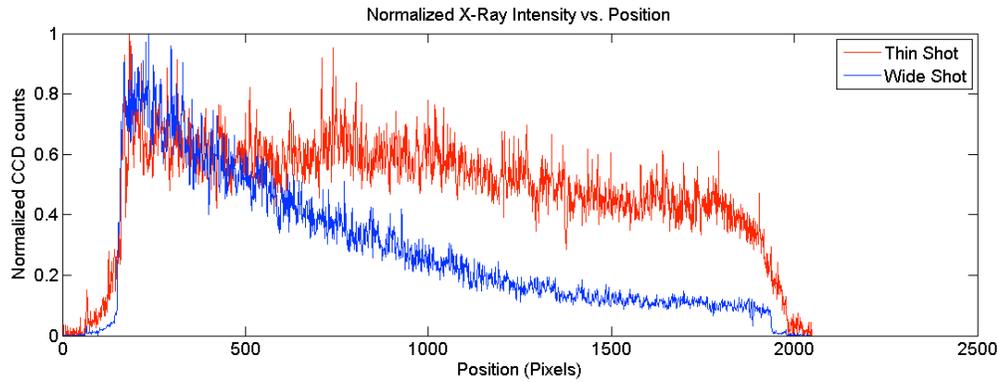
Fig. 4. Normalized X-ray Intensity vs. Position for two XRFCs on OMEGA Shot 64187
The first exposure (blue) was from a normal uniform x-ray source used in flat-fielding images. The second image (red) had a mask that only allowed a small sliver of x-ray light through (width about 1 mm reduced from 6 mm). Average x-ray intensity on the OMEGA system is approximately 700 W/cm².

Voltage reflections were also shown to occur in the simulation as seen in Fig. 5. TOAST has the ability to draw an animation of the propagating pulse as it moves through the XRFC.

Time
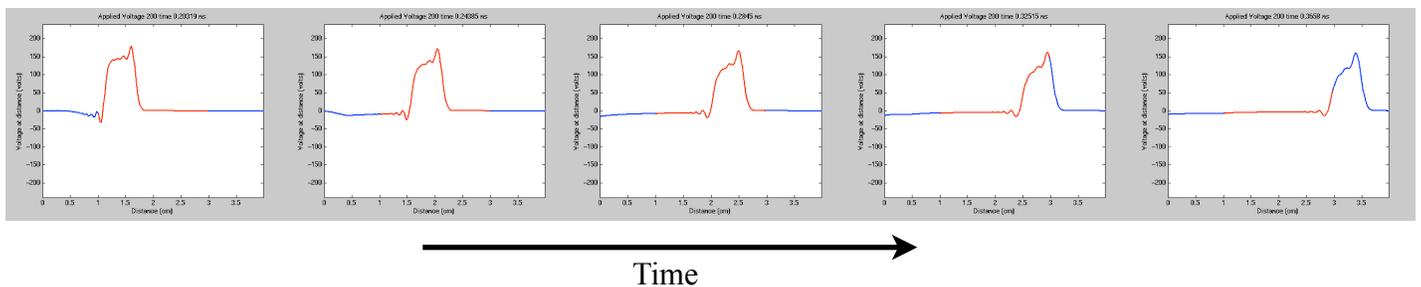
Fig. 5. TOAST Animation
These are snapshots of an animation generated by TOAST of the propagation of a voltage pulse through an XRFC. The red region is illuminated by x-rays of intensity 700 W/cm². Note the attenuation of the voltage pulse under the illuminated section of the MCP.

Voltage reflections occurred at the terminal ends of the transmission line as well as at boundaries of illuminated and non-illuminated portions of the XRFC. Higher intensity x-rays and voltage pulses produced greater reflections. The closer the terminal resistances matched the impedance of the line, the smaller the reflections were. However, reflections will always occur at boundaries between two different x-ray intensities. Figure 5 also shows significant distortion of the initial voltage pulse.

4. **Conclusion**

A one-dimensional mathematical model was produced to characterize an XRFC. The propagation of a pulse through the MCP of an XRFC was simulated using a computer program. Results indicate that the relationship between the intensity of x-rays hitting the XRFC and the signal recorded is not linear as assumed while using flat-fielding correction methods for raw XRFC images.

XRFC images are used to monitor the deformations of the shell during implosion, so one major consequence of the current method of correcting images is that the shell thickness would be inaccurately portrayed. Being able to accurately measure the shell thickness is vital in analyzing how successful certain beam configurations are for inertial confinement fusion on laser systems such as OMEGA. A potential solution for this problem would be to utilize a simulation of the XRFC such as TOAST and use as input the raw XRFC image. The outputted image would then be fed back into the program iteratively until the changes between images are minimal. Through each generation, the image will be closer to the original x-ray source.

Further research will aid in the development of the code. The goal is to incorporate other effects such as crosstalk between different sections of the XRFC itself as well as improving and adjusting models for the MCP and incoming x-rays. Running multiple instances of TOAST in parallel would potentially allow for the generation of two-dimensional images, which would provide a much more effective visualization of the interaction of the pulse with the XRFC system.

Acknowledgements

I would like to thank Dr. William Donaldson and Dr. Dustin Froula for advising and helping me with the project, Mr. Raymond Bahr for the use of a Manson source, and program director Dr. R. S. Craxton for coordinating the program for all the students involved. In addition, thanks to the Laboratory for Laser Energetics for the wonderful research opportunity.

References

[1] Gresh, Louis H. *Inertial Confinement Fusion An Introduction*. University of Rochester, Rochester. March 2009. Print.

[2] D. K. Bradley, P. M. Bell, J. D Kilkenny, R. Hanks, O. Landen, P. A Jaanimagi, P. W. McKenty, C. P. Verdon, "High-Speed Gated X-ray Imaging for ICF Target Experiments," Rev. Sci. Instrum. 63 (10), 4813-4817 (1992).

[3] "Transmission-Line Modeling of Photoconductive Switches," W. R. Donaldson and L. Mu, in /Optically Activated Switching III/, edited by R. A. Falk (SPIE, Bellingham, WA, 1993), Vol. 1873, pp. 201-207.

[4] Brophy, James J. *Basic Electronics for Scientists*. New York: McGraw-Hill Inc., 1972. Print.

[5] Wadell, Brian C. *Transmission Line Design Handbook*. Boston: Artech House Inc., 1991. Print.

[6] http://www.photonis.com/en/ism/38-longlife-micro-channel-plates.html. Web. Nov. 10, 2012.

[7] J. Kwiatkowski, F. J. Marshall, and W. Armstrong, private communication (2012).